Title

Chapter Six Raster Image Correlation Spectroscopy and Number and Brightness Analysis



Authors

Digman, Michelle A
Stakic, Milka
Gratton, Enrico

Publication Date

2013

DOI

10.1016/b978-0-12-388422-0.00006-6

CHAPTER SIX

# Raster Image Correlation Spectroscopy and Number and Brightness Analysis

**Michelle A. Digman**[*,†], **Milka Stakic**[*], **Enrico Gratton**[*,†,1]

[*]Laboratory for Fluorescence Dynamics, Department of Biomedical Engineering, University of California, Irvine, California, USA
[†]Department of Development and Cell Biology, University of California, Irvine, California, USA
[1]Corresponding author: e-mail address: egratton@uci.edu

## Contents



## Abstract

The raster image correlation spectroscopy (RICS) and number and molecular brightness (N&B) methods are used to measure molecular diffusion in complex biological environments such as the cell interior, detect the formation of molecular aggregates, establish the stoichiometry of the aggregates, spatially map the number of mobile molecules, and quantify the relative fraction of molecules participating in molecular complexes. These methods are based on correlation of fluorescence intensity fluctuations from microscope images that can be measured in a conventional laser-scanning confocal

*Methods in Enzymology*, Volume 518
ISSN 0076-6879
http://dx.doi.org/10.1016/B978-0-12-388422-0.00006-6

microscope. In this chapter, we discuss the mathematical framework used for data analysis as well as the parameters need for data acquisition. We demonstrate the information obtainable by the N&B method using simulation in which different regions of an image have different numbers of interacting molecules. Then, using an example of two interacting proteins in the cell, we show in a real case how the RICS and N&B analyses work step by step to detect the existence of molecular complexes to quantify their properties and spatially map their interactions. We also discuss common control experiments needed to rule out instrumental artifacts and how to calibrate the microscope in terms of relative molecular brightness.

## 1. INTRODUCTION

### 1.1. What can fluctuation analysis reveal about the motion and interactions of single molecules in cells?

Fluctuation analysis methods are relatively common in several areas of physics, chemistry, and biology. Fundamentally, fluctuation spectroscopy is the basis for methods such as dynamic light scattering (DLS) and fluorescence correlation spectroscopy (FCS). A major difference between DLS and FCS is that the former is applied to solutions or homogeneous samples. To generate the DLS signal, many molecules are needed. The fluctuation of the scattered lights is generated by interference among the particles. In general, DLS is used to analyze the distribution of particle sizes. Instead, FCS is sensitive to single molecules and can be applied to complex environment such as the cell interior or tissues but requires the molecules under observation to be fluorescent. Although the FCS method has some disadvantages because fluorescent molecules can bleach due to constant illumination, it can measure multiple-labeled fluorophores which is not possible in DLS. In addition, FCS has the capability to analyze the amplitude of the fluctuations and connect these amplitudes with molecular characteristics such as molecular brightness. As a result of these differences with respect to DLS, FCS has developed as an independent method during the 1970s (Magde, Elson, & Webb, 1972, 1974). A major breakthrough in the FCS approach was due to the realization that FCS measurements can be performed in live cells (Berland, So, & Gratton, 1995; Bacia and Schwille, 2003, 2007; Bacia et al., 2006; Haustein and Schwille, 2007; Kim et al., 2007; Schwille, 1999; Schwille et al., 1997a,b) and that scanning confocal microscopy methods could be exploited to obtain the map of fluctuations in entire cells and in tissues (Digman, Brown, et al., 2005; Digman, Dalal, Horwitz, & Gratton, 2008; Digman & Gratton, 2009a, 2009b; Digman,

Sengupta, et al., 2005; Digman, Wiseman, Choi, Horwitz, & Gratton, 2009; Digman, Wiseman, Horwitz, & Gratton, 2009; Ries, Chiantia, & Schwille, 2009; Ries, Yu, Burkhardt, Brand, & Schwille, 2009).

Although FCS still shares some technological and analysis approach of the DLS method, today, FCS analysis has diverged from DLS. In this contribution, we will briefly describe the conceptual advances in FCS that made possible the development of the imaging fluctuation methods, which are currently driving the research by exploiting fluctuations observed in live cellular environments for the study of molecular interactions.

## 2. A CONCEPTUAL OVERVIEW OF FLUCTUATION METHODS

The basic concept in FCS is that fluorescence intensity fluctuations in a given volume of observation are caused by single molecules or particles that randomly pass through that volume. Additional fluctuations could also arise from particles in the observation volume which change the fluorescence intensity due to conformational transitions or, in general, change their excitation–emission properties while in the observation volume. Although this is the common explanation found in almost all articles introducing FCS, this view does not convey the information about changes of the spatial location of the particle as a function of time. The consideration of the spatial distribution of molecules brings in the change of paradigm which is needed to correlate fluctuations at one location with the fluctuations in surrounding locations.

## 3. WHAT IS DIFFERENT IN THE RICS METHOD?

In classical single point FCS analysis, we consider fluctuations occurring only at one volume of illumination. In the spatial correlation approach, we consider (cross) correlations between adjacent (or far) volumes of observation. In this way, the full extent of the probability density of finding a particle at a different location and at a different time is introduced into the description of the correlation of the fluctuations. For example, if the particle diffuses isotropically, measuring the fluctuations at one point is sufficient to characterize the diffusion coefficient of the particle. However, if the particle undergoes anisotropic diffusion, the probability density of finding the particle at a given position and at a given time will depend on the position and the time. To capture the time and spatial evolution of the particle location, we need to introduce more complex correlation functions than those used in conventional FCS. In Fig. 6.1, we illustrate

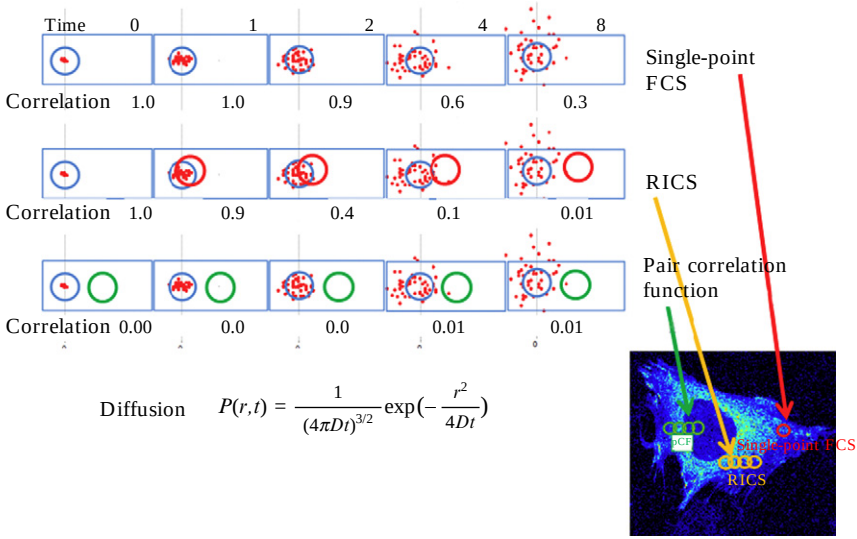


**Figure 6.1** Schematic illustration of fluctuation spectroscopy experiments. In single point FCS, the intensity fluctuations at a given observation volume are measured as a function of time due to diffusion. The correlation is the product of the intensity at time 0 (points at left in the figure) to the intensity at a later time. The correlation decreases as a function of time due to diffusion. This time depends on the diffusion coefficient of the molecule and on the size of the observation volume. In the RICS method, the position of the volume of observation is changed with time producing a correlation that is dependent on how fast molecules are moving as well as how fast the position of the volume of observation is changing with time. In the pair correlation approach, two (or more) volumes of observations are used at a given distance. Initially, a molecule is in one of the observation volume. Due to diffusion, a molecule could appear in the other volume at a later time. The time it takes to appear in the other volume depends on how fast the molecule moves, how far the two volumes are, and if there are obstacles to diffusion in between the two volumes.

the principle of the fluctuations techniques discussed in this chapter in the context of the spatial and temporal correlation due to free diffusion. The probability to find a particle at a given distance and time if the particle was at the origin at time 0 is given by the diffusion equation in Fig. 6.1 for diffusion in three dimensions. This probability can be approximated by a Gaussian in which the exponential term represents the broadening of the distribution with a variance that is function of time. The amplitude term decreases with time to maintain the integrated probability to unity.

We set the probability to be unity at time $t=0$ in the volume of observation. In the first row (Fig. 6.1), we schematically show the experiment for

the single point FCS experiment. The volume of observation is always the same in this approach. As the time evolves, the probability distribution broadens. At some point in time, the particle has a probability to be found outside the volume of observation (the blue circle in first row of Fig. 6.1). The correlation function implicitly defined in the figure as the product of the number of particles inside the blue circle at time 0 and the number of particles in the blue circle at a later time has the property that the correlation decreases as a function of time since the particle can be found everywhere in the volume. We normalize the correlation function so that the correlation goes to zero at very long time when the probability of finding a particle in a given volume is equal everywhere.

Row 2 of Fig. 6.1 shows the RICS approach. The RICS correlation function is calculated assuming that the position of the volume of observation changes with time according to a specific relationship. This relationship is typically obtained when a raster scan is done as in the common laser-scanning microscope. The position along the horizontal direction changes linearly with time with a characteristic motion given by the linear motion of the scanner. The laser scan speed and pixel size can be manually adjusted. In the vertical direction, the motion is also linear, but the speed of the motion depends on the line time.

Row 3 of Fig. 6.1 shows the pair-correlation function approach. In this method, the probability distribution is sampled simultaneously at two different positions. If the two positions are nonoverlapping, the same particle cannot be found in the two separated locations. Only after some time when the distribution has sufficiently broadened, the same particle can be observed at the second location. The time cross-correlation of the intensity fluctuations at these two locations provides information about the average time to go from one location to the other. Using this approach is possible to explore the probability distribution in a very large volume. The pair-correlation approach gives similar information of the single particle-tracking method but using many particles simultaneously and without the requirement of observing separated particles (Digman & Gratton, 2009b).

## 4. RICS AND CROSS-RICS

The RICS and ccRICS correlation functions are shown below

$$G_{\mathrm{RICS}}(\xi,\psi)=\frac{\langle I(x,y)I(x+\xi,y+\psi)\rangle}{\langle I(x,y)\rangle\langle I(x,y)\rangle}-1 \qquad [6.1]$$

$$G_{\text{ccRICS}}(\xi,\psi) = \frac{\langle I_1(x,y) I_2(x+\xi, y+\psi)\rangle}{\langle I_1(x,y)\rangle \langle I_2(x,y)\rangle} - 1 \qquad [6.2]$$

where $I$ is the intensity at each pixel and the brackets indicate the average over all pixels $x$, $y$ of an image. The indices 1, 2 indicate channel 1 and channel 2, respectively. As the correlation functions above show, one image is sufficient to determine the RICS correlation function. However, in general, a stack of images is collected with the purpose of separating the mobile from the immobile population of molecules.

The definition of the RICS correlation function is identical to the definition of the image correlation spectroscopy (ICS) given by Petersen et al. (Petersen, 1986; Petersen et al., 1998; Petersen, Höddelius, Wiseman, Seger, & Magnusson, 1993). The difference in the RICS approach is in the way data are collected in the raster scan confocal microscope. There is a relationship between the position of the pixel in the image and the time the pixel is measured.

$$\text{time at pixel } n = y \times \tau_l + x \times \tau_p \qquad [6.3]$$

$$\xi = x \times \tau_p \qquad [6.4]$$

$$\psi = y \times \tau_l \qquad [6.5]$$

The resulting correlation function can then be expressed in terms of the pixel time $\tau_p$ and the line time $\tau_l$.

In relation to Fig. 6.1, it is clear that if the pixel dwell time is very long a molecule could move faster than the scanner when the collection of the line is finished. In this case, fast molecules could not contribute to the correlation function. If this occurs, the diffusion obtained by the RICS analysis will be smaller than the true diffusion coefficient. Also, the amplitude of the correlation function will be smaller because the numerator of Eq. (6.2) will be smaller but the denominator will be the same.

Therefore, it is important that the pixel time to be fast enough and the pixel size to be sufficiently larger to "catch" the molecules before the line return will occur. Figure 6.2 shows the relation between the required pixel dwell time and the diffusion coefficient. For common situations, for example, for a protein diffusing in a cell with a diffusion coefficient of 20 $\mu m^2/s$, a pixel size of 0.05 μm and using a relatively slow pixel dwell time (25 μs), the condition for "catching" the molecules occur at about pixel 2–3. This discussion shows that the RICS analysis can be done using small subframes (e.g., 16 pixels) which correspond to averaging the diffusion coefficient in a

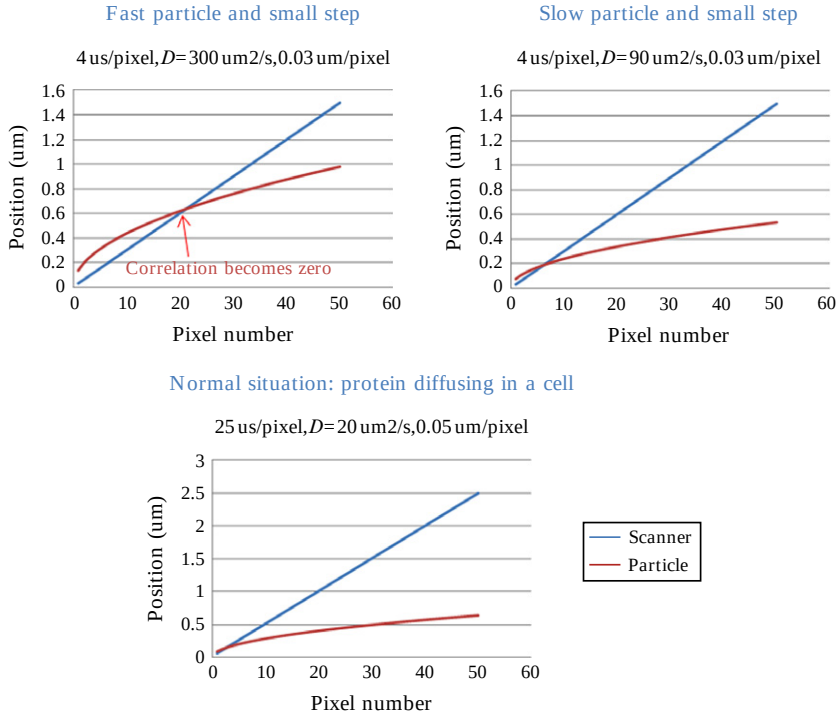


**Figure 6.2** Schematic representation of timing relationships in the RICS method. The horizontal axis (pixel) is scanned linearly with time. The position of a diffusing particle changes with the square root of time. At some time (or pixel), the scanner will have traveled a larger distance than the particle. At that time (or pixel distance), the correlation according to Fig. 6.1 goes to zero. This is the minimum number of pixels needed to compute the correlation function. This number of pixels depends on the pixel size, the scan speed, and the diffusion coefficient of the molecule.

region of about 0.8 μm. This is the typical "spatial" resolution of the RICS method which is larger than the size of a diffraction limited spot but no so large that it only gives averages over the entire cell.

In the example below, we show how to produce maps of diffusion and ($G_0$) for a cell expressing EGFP–paxillin. The focal adhesions where paxillin concentrate are visible as areas of relatively large intensity. The image was sequentially analyzed using small regions of analysis (32 pixels) at a time. The apparent diffusion is larger in the regions away from the focal adhesions (Fig. 6.3 Panel D). For this measurement, the spatial resolution of the diffusion parameter map was 1.6 μm.

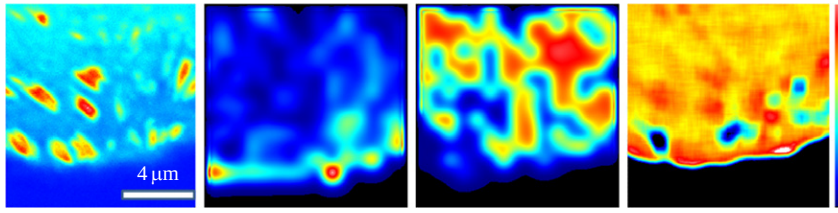


**Figure 6.3** Intensity image, (*G*0) map, Diffusion map and brightness map of paxillin–EGFP in focal adhesions. The same color scheme at right is used for all figures. The corresponding full scale are intensity 0–489 photon/s; $G(0) = 0.0064$, $D = 0$–46 $\mu m^2/s$, 28,000–52,000 counts/dwell time/molecule. The maps from the fluctuation experiments were obtained using a region of analysis of 32 pixels and sliding this region in steps of 16 pixels across the entire image.

## 5. PCH AND AMPLITUDE FLUCTUATION ANALYSIS

As we discussed in the previous section, in a fluctuation experiment, there is a time correlation between fluctuations at different locations and at different times. In addition, the amplitude of the fluctuations contains information about the brightness of the particle. To extract this information, we analyze the statistics of the fluctuation amplitude using different mathematical methods. The PCH (photon counting histogram) method was introduced in 1999 (Chen, Müller, So, & Gratton, 1999). This method is based on measuring the photon counting distribution at one location, similar to the single point FCS experimental approach. This method is quite powerful since the photon counting distribution can provide information about the brightness and the number of particles in the volume of observation. However, when analyzing images, the limited statistic available at each pixel does not allow the full photon counting distribution to be analyzed. Instead, for the analysis of images, we use a method that utilizes only the first and second moment of the histogram of the amplitude fluctuations. This method is called the Brightness and Number analysis or N&B (Digman et al., 2008). In this original presentation of the method, the basic of the moment analysis was presented. In a subsequent paper {Digman, 2009 #68}, the concept of cross-correlation based on the brightness of complexes using proteins with two fluorescent labels was introduced. The analysis of the cross-brightness of the complex leads the method to determine the stoichiometry of the complex. The stoichiometry is determined by first "isolating" the particles that

are cross-correlated and then analyzing the brightness of the complex in terms of how bright are the cross-correlated species in each color. However, in the 2009 article {Digman, 2009 #68}, the determination of the number of molecules in the complex with respect to the molecules of each species in the cell was not discussed. In this chapter, we present the equations needed to perform the cross-number analysis and we provide an example of a biological system in which a complex is formed and the fractional number of molecules in the complex is calculated.

## 6. N&B AND CROSS-NB

The data set need for the Number and Brightness analysis consists of a stack of images of the same field of view observed at two different emission band-passes if cross-N&B measurements are required. For each pixel of the stack of images, we define

$$\mathrm{av} = \frac{\sum_k I(x,y)}{K} \quad [6.6]$$

$$\mathrm{var} = \frac{\sum_k (I(x,y) - \mathrm{av})^2}{K} \quad [6.7]$$

$$\mathrm{cross\_var} = \frac{\sum_k (I_1(x,y) - \mathrm{av}_1)(I_2(x,y) - \mathrm{av}_2)}{K} \quad [6.8]$$

Where the sum is over the same pixel in each frame of the stack, $K$ is the number of frames and $I$ is the intensity at one pixel of each frame

$$B_1 = \frac{\mathrm{var}_1}{\mathrm{av}_1}, \quad \text{Brightness of channel 1} \quad [6.9]$$

$$B_2 = \frac{\mathrm{var}_2}{\mathrm{av}_2}, \quad \text{Brightness of channel 2} \quad [6.10]$$

$$B_{cc} = \frac{\mathrm{cross\_var}}{\mathrm{av}_1 \times \mathrm{av}_2}, \quad \text{Cross\_variance} \quad [6.11]$$

$$N_1 = \frac{\mathrm{av}_1^2}{\mathrm{var}_1}, \quad \text{Number of particles in channel 1} \quad [6.12]$$

$$N_2 = \frac{\mathrm{av}_2^2}{\mathrm{var}_2}, \quad \text{Number of particles in channel 2} \quad [6.13]$$

$$N_{cc} = \mathrm{cross\_variance}, \quad \text{Cross number} \quad [6.14]$$

$$\frac{N_{cc}}{N}, \quad \text{Fraction of cross number} \quad [6.15]$$

The equations for the relative fraction of cross-correlated molecules have not been given before in the context of the N&B technique. They follow the same concept used in the single point cross-correlation fluctuation spectroscopy equation to determine the fraction of cross-correlated molecules. A new concept in the cross-correlation N&B analysis is the stoichiometry contour map, which provides the most common brightness composition of molecular complexes found in a sample. To show the utility of the stoichiometry map, let us consider a situation in which we detect two species in two separate channels, for example, green and red. The two species can form a complex in which two molecules of the red species associate with one green molecule. From the point of view of the green channel, the brightness of all components is the same. In the red channels, some of the molecules will appear brighter in the complex. The individual brightness map cannot reveal the nature of the complex. The Bcc histogram (Eq. 6.11) will tell us that there is a positive cross-correlation, but this histogram alone cannot reveal the composition of the complex. To construct the stoichiometry histogram, we scan all pixels that have a positive cross-brightness signal and we detect the individual brightness at the two channels for that pixel. We then construct the histogram of the brightness of the two channels with the condition that they have to be cross-correlated. The brightness of each channel is normalized to the molecular brightness of each species. Using this normalization, we can determine the molecular composition of the complex.

## 7. SIMULATIONS FOR CROSS-RICS AND CROSS-N&B

In the following, we show simulations of molecules interacting in different number at selected spots of an image (Fig. 6.4). With simulations we can better determine if the algorithms we are using can recover the underlying molecular distributions. For this part, we are using simulated data in which the image is divided in spots with different ratio of cross-correlated molecules according to Table 6.1. This table describes the number of molecules in the various spots of the image according to the simulation and their properties. All molecules diffuse with the same diffusion coefficient of $D = 10\ \mu m^2/s$.

All molecules have the same brightness. Channel 1 has constant number of molecules (100) in each spot but variable number of cross-correlated molecules. Channel 2 has a variable number of molecules, and all of them (100%) correlate with a variable fraction of the molecules in channel 1, depending on the spot. Table 6.1 shows, for each of the eight spots, the expected

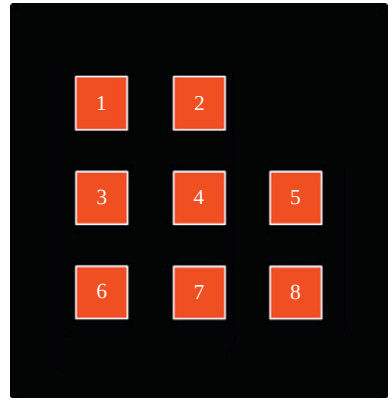


**Figure 6.4** Definition of the spot number locations for Table 6.1 and Figs. 6.5 and 6.6.

**Table 6.1** Intensity, Number and Brightness values for the 8 spots of the simulation

| Spot | Channel 1 | Channel 2 | av1 | av2 | B1 | B2 | N1 | N2 | Ncc | Ncc/N1 | Ncc/N2 |
|---|---|---|---|---|---|---|---|---|---|---|---|
| 1 | 100 + 0 | 0 | 100 | 0 | 1 | 0 | 100 | 0 | 0 | 0 | 0 |
| 2 | 90 + 10 | 10 | 100 | 10 | 1 | 1 | 100 | 10 | 10 | 0.1 | 1 |
| 3 | 80 + 20 | 20 | 100 | 20 | 1 | 1 | 100 | 20 | 200 | 0.2 | 1 |
| 4 | 70 + 30 | 30 | 100 | 30 | 1 | 1 | 100 | 30 | 30 | 0.3 | 1 |
| 5 | 60 + 40 | 40 | 100 | 40 | 1 | 1 | 100 | 40 | 40 | 0.4 | 1 |
| 6 | 50 + 40 | 50 | 100 | 50 | 1 | 1 | 100 | 50 | 50 | 0.5 | 1 |
| 7 | 40 + 60 | 60 | 100 | 60 | 1 | 1 | 100 | 60 | 60 | 0.6 | 1 |
| 8 | 0 | 100 | 0 | 100 | 0 | 1 | 0 | 100 | 0 | 0 | 0 |

intensities, relative brightness, and number of molecules for both channels for this simulation as well as the number of cross-correlated molecules. Figure 6.5 shows the result of the analysis of the above simulations obtained with the SimFCS software (available at www.lfd.uci.edu). The brightness map for the two channels shows that molecules have the same brightness in the two channels, although each spot has a different intensity in channel 2. Accordingly, the number map is different for the two channels and obviously in this example follows the intensity map.

Next in Fig. 6.6, we show the brightness maps of the molecules that are cross-correlated and the map of the fractional number of the cross-correlated

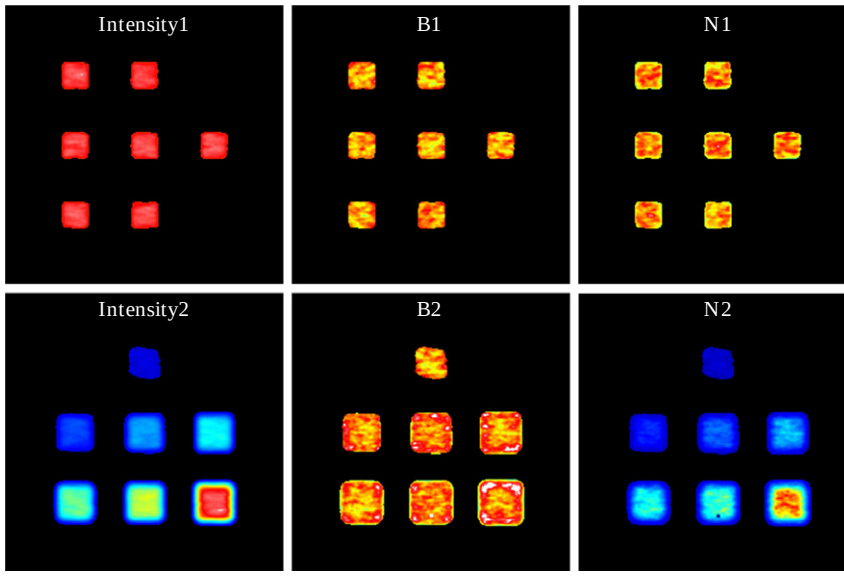


**Figure 6.5** According to expected values from Table 6.1, we recover a uniform intensity in all spots for intensity 1, a variable intensity for the spots as seen in channel 2, the same brightness in all spots for channel 1 and channel 2, the same number of molecules for channel 1 in all spots, and a variable number of molecules in the various spots for channel 2.

molecules. The Bcc map (cross-brightness) shows the same cross-brightness in each spot, since all molecules that are cross-correlated have the same brightness. The stoichiometry map shows that there is only one cross-correlated population with a ratio 1:1 of the two molecules. The number of cross-correlated molecules instead is different in the different spots in channel 1 but is the same in each spot of channel 2. The value of the fraction of molecules recovered by this algorithm is identical to the fraction of molecules simulated.

## 8. APPLICATIONS OF RICS AND N&B TO DETECT MOLECULAR COMPLEXES IN CELLS

In this section, we show an application of the cross-RICS and cross-N&B using a biological system in which two proteins are known to interact. T3T cells were co-transfected with dynamin-2a and endophilin (see Section 12 at the end of this chapter). What is known for this system is that the two proteins, dynamin-2a labeled with EGFP and endophilin

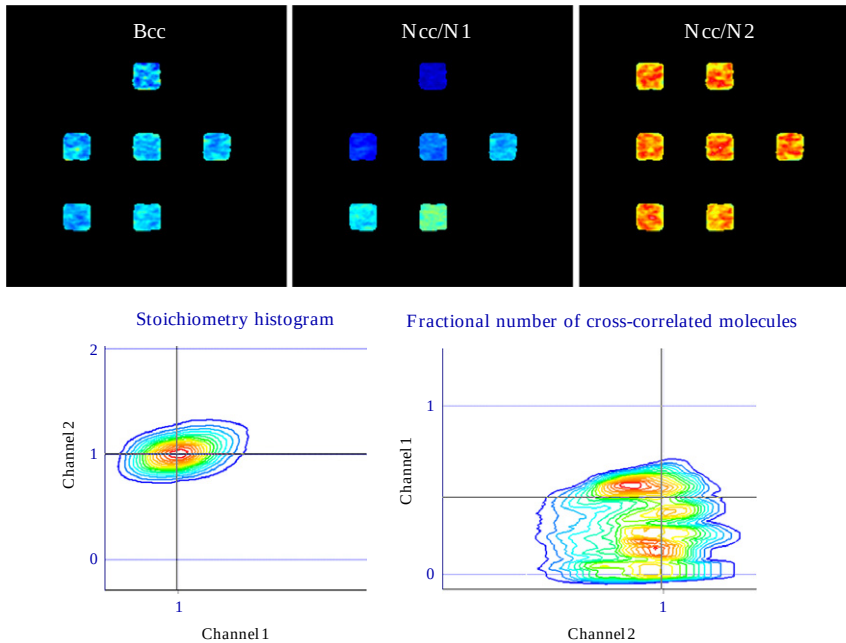


**Figure 6.6** The cross-brightness is the same for all molecules since the molecules that are in the complexes have all the same brightness. The ratio of molecules that are in the complex with respect to the total molecules in each channels varies in channel 1 in the different spots, but it is the same (all molecules are cross-correlated) in channel 2. The stoichiometry histogram reports the relative number of molecules of each kind in the complex. In this case, all the complexes have a stoichiometry 1:1. The histogram of the fractional number of cross-correlated molecules varies only along the channel 1 axis, since all the molecules in channel 2 are cross-correlated.

labeled with mCherry should form a complex in the cytoplasm (Ross et al., 2011; Sundborger et al., 2010). Endophilin in the cytoplasm has been found to be a dimer (Ringstad, Nemoto, & De Camilli, 2001; Ross et al., 2011).

We measured the correlation between the two proteins in the cytoplasm. The intensity image shows that the dynamin-2a is concentrated in small vesicles while endophilin is more uniformly distributed in the cytoplasm (Fig. 6.7A and C). First, we perform the RICS analysis to determine if there are mobile molecules that can be detected in the two channels and if they are cross-correlated (Fig. 6.7B and D). The RICS analysis only reports on the mobile molecules. Immobile structures or slowly moving vesicles do not contribute to fast molecular fluctuations. Vesicles carrying both colors are clearly cross-correlated when they move. We eliminate these large particles

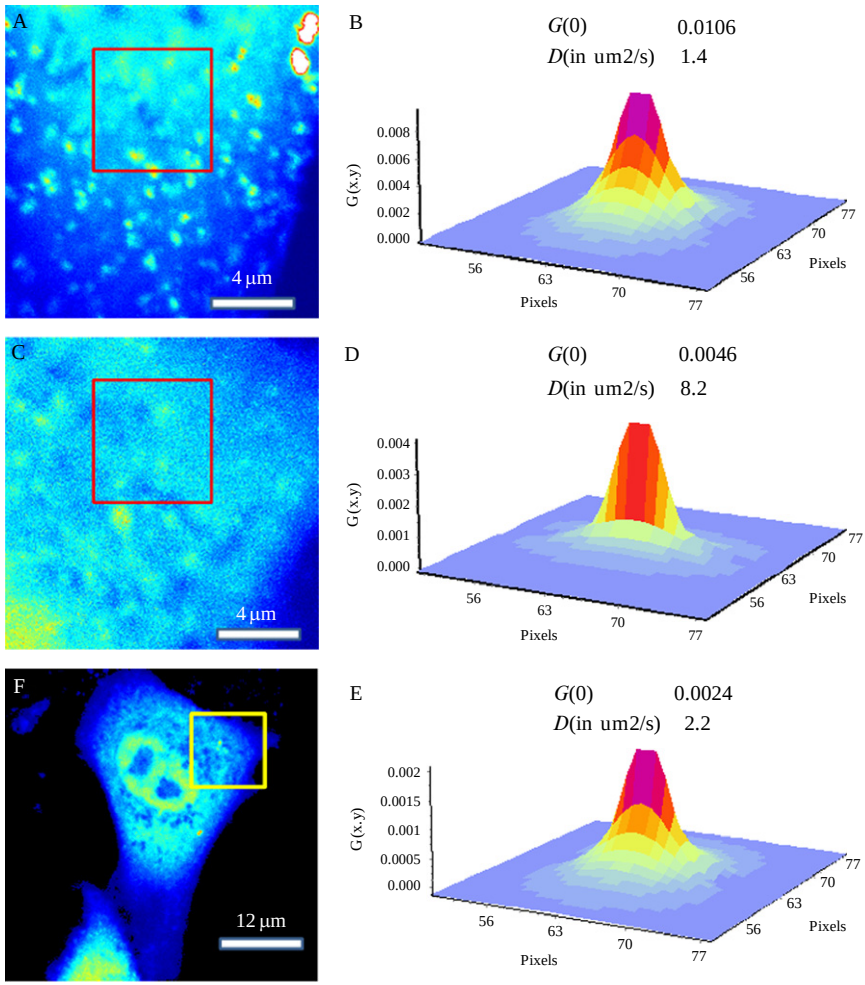


**Figure 6.7** Cell co-expressing dynamin2a-EGFP and endophilin-mCherry. Pixel size is 0.065 µm. Optical section in the cytoplasm. Only the part in the red square was used for the RICS analysis. (A) Channel 1 (EGFP) and (C) Channel red (mCherry). (B and C) RICS autocorrelation function and fit using one component diffusion for the green and red channels, respectively. (E) RICS cross-correlation. For the fit, the waist was measured to be 0.23 µm. The same waist was used for both wavelengths. (F) Unzoomed average intensity image of the red channel. The area analyzed in parts A–E is in the yellow square.

in our analysis using the moving average method (Digman et al., 2005b). In both channels, we find mobile molecules. The recovered diffusion coefficients for the individual channels are reported in the RICS analysis of Fig. 6.7. We then analyze this image for cross-correlation between the

two proteins. We found that the two proteins cross-correlate, although the coefficient of cross-correlation is relative small (Fig. 6.7E). We then calculate the map of the brightness in the two channels (B1 and B2, Eqs. 6.9 and 6.10) (Fig. 6.8). For dynamin2a, the molecular brightness corresponds to the monomer. This is determined by a calibration procedure using cells expressing only EGFP (Fig. 6.9). For four different cells and several focal planes in the cytoplasm of each cell, we found a relatively narrow distribution of the average brightness for dynamin2a-EGFP, which correspond to the EGFP monomer.

The average brightness of endophilin in the cytoplasm is higher than the brightness expected for a monomer of mCherry (Fig. 6.9) and its value better match that of a dimer in accord with previous results (Ross et al., 2011). We then calculated the brightness of the molecules that cross-correlate using the Bcc (brightness cross-correlation algorithm, Fig. 6.8D). Using the values of

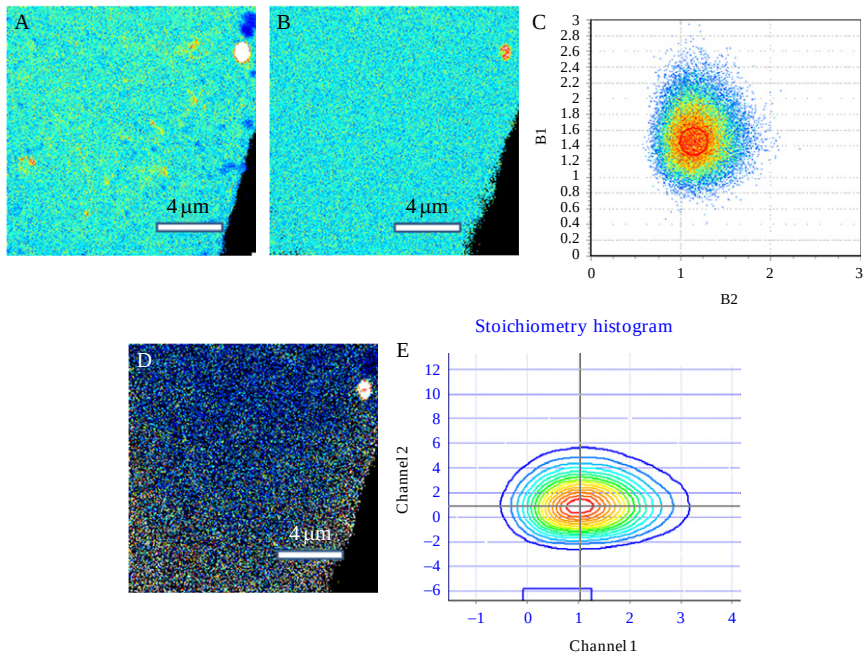


**Figure 6.8** Brightness analysis of the cell shown in Fig. 6.7. (A) Green channel. (B) Red channel. (C) 2-dimensional pixel histogram of the values of brightness for the two channels. The *x* and *y* numbers above are used for the calibration of the brightness of mCherry and EGFP, respectively. (D) Cross-correlation brightness map. (E) Contour map of the number of pixels in channel 1 of a given brightness which cross-correlate with channel 2 for all possible brightness. This is the so-called stoichiometry histogram. In this case, the most abundant value is at a ratio 1:1.

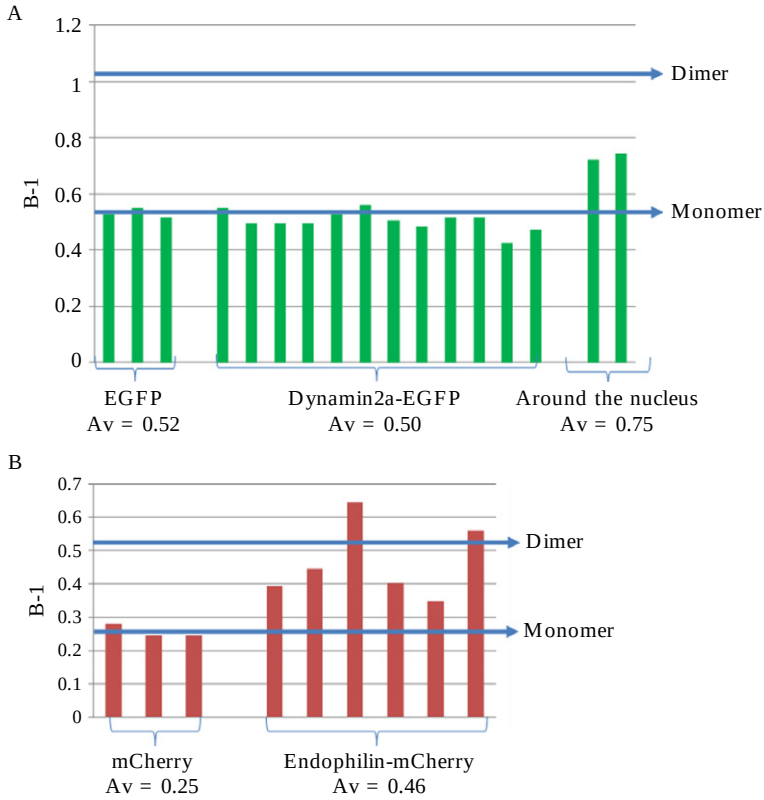


**Figure 6.9** Calibration of (A) the EGFP and (B) mCherry channel. Three cells expressing EGFP and mCherry were used to calibrate the brightness scale. The plane of focus was in the cytoplasm of the cells. For the dynamin2a-EGFP, four cells were measured with the plane of focus on the cytoplasm for a total of 12 planes. All cells and planes show the same brightness than for the EGFP only cell. For the same, four cells for a total of six focal planes in the cytoplasm of cells expressing the endophilin-mCherry show larger brightness than the mCherry alone, in the range expected for a dimer of the endophilin protein in accord with previous results. The brightness scale is in units of counts/dwell time/molecule where the dwell time was 12.6 μs.

Bcc and B1-B2, we construct the average stoichiometry histogram which is about one endophilin per dynamin-2a. This observation was not previously reported. The results are interesting for the understanding of the role of dynamin2a and endophilin in the cytoplasm of cells, but we caution that only four cells were analyzed for determining the stoichiometry of this cytoplasmic complex. Since there is an unknown fraction of endogenous material, in these type of experiments, we need to measure many cells to

explore a range of concentrations to avoid conclusions based perhaps on a largely under or over expressing cell. At present, it is unclear how a species that appears to be a dimer could form a complex as a monomer. However, we note that the fraction of molecules in the complex is a small fraction of the total molecules.

The Number analysis shows that there are more molecules of dynamin-2a than endophilin by about a factor of 3–4 (Fig. 6.10).

About 36% of the total endophilin molecules are in a complex with dynamin-2a, but less than 12% of the total dynamin-2a molecules are in the complex. In other words, there is an abundant pool of dynamin-2a in the cytoplasm which is not cross-correlating with endophilin. This is in agreement with the ccRICS analysis which shows also about 50% of

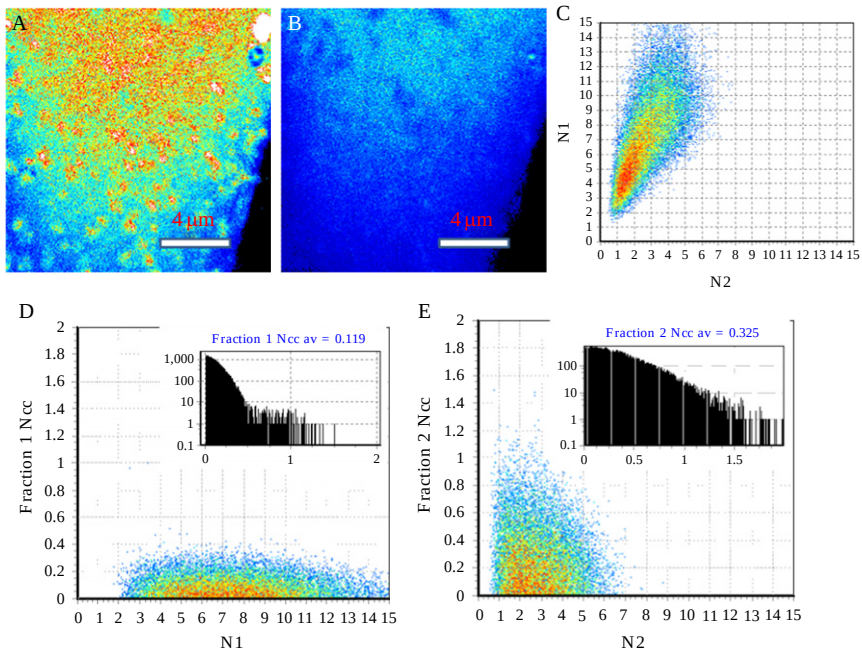


**Figure 6.10** Number analysis of the cell shown in Fig. 6.7. (A) Number of particles in the green channel. (B) Number of particles in the red channel. (C) Two-dimensional pixel histogram of the values of the number of particles for the two channels. The *x* and *y* numbers above are used for the calibration of the maximum number of particles of mCherry and EGFP, respectively. (D) Fraction of molecules cross-correlated in channel 1. The inset is the histogram. (E) Fraction of molecules cross-correlated in channel 2. The inset is the histogram.

endophilin and 24% dynamin-2a in the complex. The difference between the two estimates could arise from the fact that the ccRICS analysis which calculates the fraction of the mobile complexes with respect to the total mobile molecules while the number analysis calculates the ration between the cross-correlated molecules to the total number of molecules, mobile, or not.

## 9. CALIBRATION MEASUREMENTS USING EGFP AND mCHERRY AND EFFECTIVE BLEEDTHROUGH

We calibrated the brightness scale using a cell expressing only EGFP (Fig. 6.9). We found that EGFP has a B value of 0.55 and mCherry was 0.25 (Fig. 6.9). Remember that the B value is 1 plus the molecular brightness in units of counts/dwell time/molecule. In the sample with EGFP-only, we also estimated the amount of bleedthrough to the red channel. We found that brightness of the EGFP in the red channel was $B = 0.028$, which is about 11% of the brightness of mCherry.

## 10. DIFFERENCE OF DISTRIBUTION IN THE NUCLEUS VERSUS CYTOPLASM OF DYNAMIN-2A

For this demonstration, we selected a bright cell, presumably overexpressing both proteins. The reason for using overexpressing cells in this example is to avoid interference with the endogenous population. For the purpose of this demonstration of the method, it is instructive to have an excess of the labeled proteins. Of course from the biological point of viewpoint, overexpressing cells could behave very differently than wild-type cells. For the overexpressing cells, we found that dynamin-2a tends to be less concentrated in the nucleus but with a high concentration in the perinuclear region. Instead, endophilin distributes equally in the nucleus and in the cytoplasm. For this example, we would like to establish whether or not there is association between the two proteins in the nucleus where the concentration of dynamin-2a is very different than in the cytosol. Furthermore, our relative fraction analysis should give the information about the relative number of molecules (concentrations) in the various cell compartments and the fraction of molecules in the aggregates.

Figure 6.10 shows the intensity images in the two channels where there is a large difference for the EGFP channel indicating the relative low

concentration of the dynamin-2a in the nucleus. The brightness map is relatively uniform, compared to the intensity analysis. The brightness analysis shows that on the average, the increased brightness of the dynamin-2a in the perinuclear region is due to aggregates of about two to four dynamin-2a molecules. This could be due to bleedthrough of the high brightness of the vesicles into the surrounding cytoplasmic compartment rather than truly cytoplasmic proteins. In principle, everything that is immobile should give a value of $B=1$. However, if there is a relatively fast moving pool of vesicles, then the moving average filtering algorithm used to compensate for slow moving components will not be able to completely remove them. Instead, the brightness of the endophilin is uniform in the entire cell and corresponds to the brightness of the dimer (Fig. 6.10). Also for this overexpressing cells, we found that stoichiometry of the complex is 1:1 in the nucleus (Fig. 6.11).

In regard to the number analysis, we first show the map of the number of molecules in the two channels. Clearly, there is a large change in the number of molecules in channel 1 in the perinuclear region but very few in the nucleus. When we analyze for the cross-correlated molecules, we find them everywhere. However, we can see that the fewer molecules of dynamin-2a in the nucleus are in percentage more cross-correlated than the large pool of dynamin2a in the cytoplasm. On the contrary, since there is an excess of endophilin in the nucleus, the measured fraction of interacting molecules for endophilin is smaller in the nucleus (Fig. 6.12).

## 11. CONCLUSIONS AND FUTURE PROSPECTS

In this method article, we discuss the RICS and N&B methodology used to measure the diffusion of single molecules in cells and their aggregation from a stack of raster scan images. The RICS and the N&B methods were first proposed few years ago. In this contribution, there is an original new addition to the number analysis with the introduction of the concept of number of cross-correlated molecules. The cross-correlation is detected by the simultaneous appearance of fluctuation in the same pixel of an image. The concept is similar to the cross-correlation of fluctuations used in fluctuation correlation spectroscopy. Here, instead of measuring the fluctuation in a single point, we use a stack of raster scan images and we detect correlation of fluctuations in every pixel of an image. By correlating the fluctuations

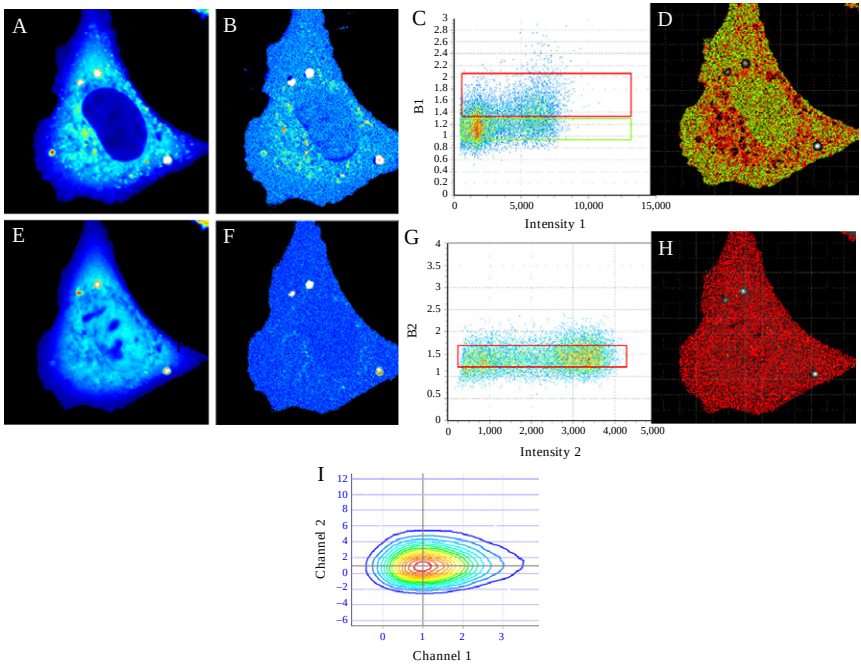


**Figure 6.11** Cell over expressing dynamin2a and endophilin. (A) Intensity image of green channel. (B) Brightness map of the green channel. (C) Selection map, green cursor corresponds to the brightness of monomers, and red cursor corresponds to higher aggregates. (D) Selection map coded with the color of the cursors in (C). (E) Intensity image of red channel. (F) Brightness map of the red channel. (G) Selection map, red cursor corresponds aggregates of 2 endophilin molecules. (H) Selection map coded with the color of the cursors in (G). (I) Stoichiometry map showing that the most populated species is the 1:1 molecular complex.

among pixels and among frames in the stack, we obtain information about the diffusion of molecules, the number of fluorescent molecules in a pixel, and their brightness. The cross-correlation of fluctuations between two molecular species emitting in two different channels gives us information about their interactions, the stoichiometry of the molecular aggregate, and the fraction of molecules interacting of each independent species. The method of data analysis makes use of fast Fourier transform algorithm which result is a very fast computation and quasi real-time display. Data are collected using commercial laser-scanning microscope without any change in the hardware and optics.

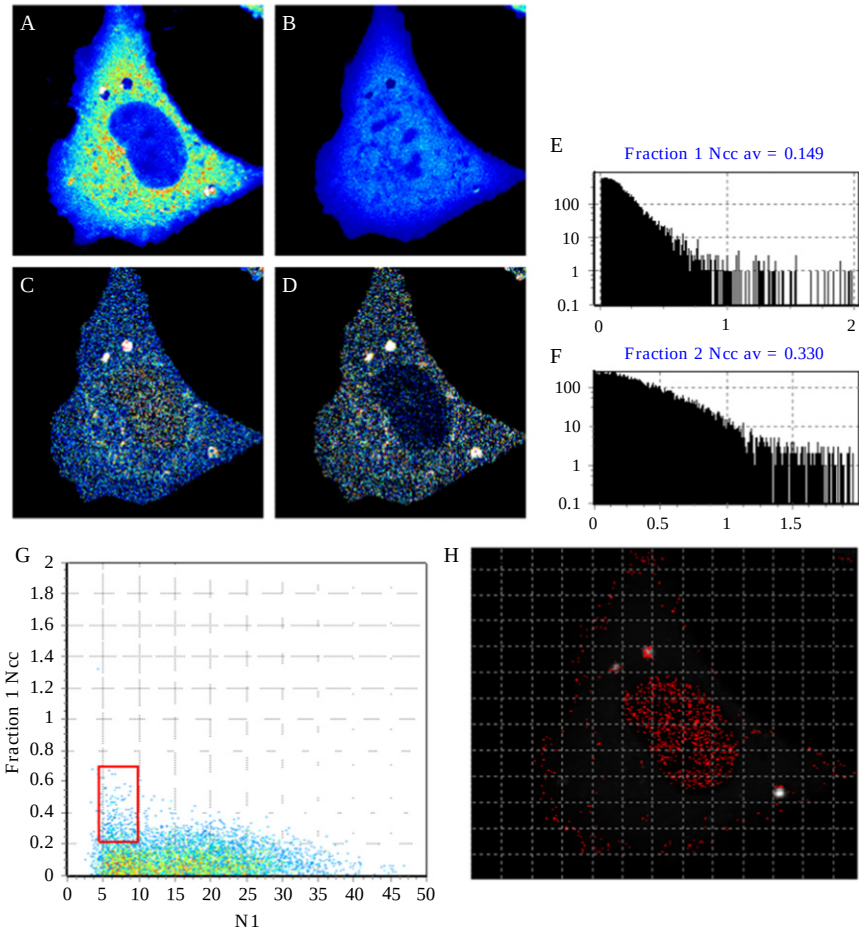


**Figure 6.12** Cross-number analysis of the cell showing in Fig. 6.11. (A) and (B) fluorescence intensity in the green and red channels, respectively. (C) and (D) Cross-number maps for the green and red channels, respectively. The scale in the figure is obtained from the histograms in (E) and (F), for the two channels. (G) Selection of the Ncc1 versus N1 histogram for low number N1 (in the nucleus) has the larger fraction of cross-correlated molecules. The region selected by the pixels in the red square is shown in panel H.

With the recent introduction of very fast and sensitive cameras based on the cMOS technology, the fluctuation methods could be used with these parallel detectors, potentially improving by order of magnitude the speed of data acquisition.

## 12. MATERIALS AND METHODS

### 12.1. NIH3T3 cell cultures

NIH3T3 cells were grown in High Glucose Dulbecco's Modified Eagle Medium (DMEM) (Invitrogen, Carlsbad, CA) supplemented with 10% FBS and 1× pen/strep at 37 °C in a humidified 5% $CO_2$ incubator. Twenty-four hours prior to imaging cells were plated at 50–80% confluency in a pre-coated fibronectin [2 mg/ml] 35-mm glass bottom dish (No. 1.5, 0.17 mm thickness) (MatTek Corp, Ashland, MA). Cells were transfected with 0.4–1 μg of DNA and Lipofectamine(tm) 2000 Reagent according to manufacturer's protocol (Life Technologies, Grand Island, NY).

### 12.2. One-photon microscopy, RICS, ccRICS, N&B, and ccN&B acquisition

All cells were imaged using an Olympus FV1000 inverted laser-scanning confocal microscope using a 60× 1.2NA water UPlanSApo objective (Olympus America Inc.). To insure cell viability during the course of the experiments, a humidified stage top incubation chamber set to 37 °C with an objective warmer was mounted (Tokai Hit Co., Ltd.) and allowed to stabilize for 20 min before each plate was imaged. EGFP and mCherry were excited with an Argon Ion laser set to 488 nm (1% percent) and a 559-nm diode laser (1% percent), respectively. The 405/488/559/635 primary dichroic filter was selected. Band pass filters at 505–540 and 575–675 nm were configured for green and red emission, respectively. Images were collected at 12.5 μs/pixel at 256 × 256 pixel resolution with a scanning areas ranging from 70 × 70 μm to 16 × 16 μm using the photon counting mode of the Olympus FV1000 microscope. For the raster image correlation spectroscopy (RICS) acquisition, the zoom was set to 50 nm/pixel (zoom 16.5) at 256 × 256 image resolution. In all experiments, a stack of 100 frames was collected with a frame time of 1 s. The parafocal illumination of the two colors was determined using 40 nm yellow-green beads. The $x$–$y$ and $z$ illumination volumes were coincident in the two colors within 20 nm.

### 12.3. Data analysis

All data analyses were performed using the SimFCS program (available at www.lfd.uci.edu). For the RICS analysis, correction for cell and organelles motions was achieved using a moving average of 10 frames. This method

effectively removes every motion occurring in times longer than 10 s. Bleaching was checked for each measurement. Bleaching never exceed 10% of the original intensity. The RICS analysis is independent form bleaching since the correlation is calculated for each frame. Instead for N&B analysis, a change of 10% of the average intensity can result in substantial artifacts. We apply the pixel detrend routine of SimFCS for random counts using a section of 10 s. Since this procedure slightly modifies the brightness calibration, for ach measurement, we recalibrate internally the S factor of the SimFCS program. This factor must be such that a part of the sample that is immobile must have a brightness of 1. In every field, we imaged a part of the support glass and we modified the value of S to achieve a B value of 1 in that region of the image. Using this procedure, we obtained very consistent results.

## ACKNOWLEDGMENTS

Funds were provided by NIH Grants P41-RR03155, P41 GM103540, and P50 GM076516.

## REFERENCES

Bacia, K., & Schwille, P. (2003). A dynamic view of cellular processes by in vivo fluorescence auto- and cross-correlation spectroscopy. *Methods*, *29*, 74–85.

Bacia, K., Kim, S. A., & Schwille, P. (2006). Fluorescence cross-correlation spectroscopy in living cells. *Nature Methods*, *3*, 83–89.

Bacia, K., & Schwille, P. (2007). Practical guidelines for dual-color fluorescence cross-correlation spectroscopy. *Nature Protocols*, *2*, 2842–2856.

Berland, K. M., So, P. T., & Gratton, E. (1995). Two-photon fluorescence correlation spectroscopy: Method and application to the intracellular environment. *Biophysical Journal*, *68*, 694–701.

Chen, Y., Müller, J. D., So, P. T., & Gratton, E. (1999). The photon counting histogram in fluorescence fluctuation spectroscopy. *Biophysical Journal*, *77*, 553–567.

Digman, M. A., Brown, C. M., Sengupta, P., Wiseman, P. W., Horwitz, A. R., & Gratton, E. (2005). Measuring fast dynamics in solutions and cells with a laser scanning microscope. *Biophysical Journal*, *89*, 1317–1327.

Digman, M. A., Dalal, R., Horwitz, A. F., & Gratton, E. (2008). Mapping the number of molecules and brightness in the laser scanning microscope. *Biophysical Journal*, *94*, 2320–2332.

Digman, M. A., & Gratton, E. (2009a). Analysis of diffusion and binding in cells using the RICS approach. *Microscopy Research and Technique*, *72*, 323–332.

Digman, M. A., & Gratton, E. (2009b). Imaging barriers to diffusion by pair correlation functions. *Biophysical Journal*, *97*, 665–673.

Digman, M. A., Sengupta, P., Wiseman, P. W., Brown, C. M., Horwitz, A. R., & Gratton, E. (2005). Fluctuation correlation spectroscopy with a laser-scanning microscope: Exploiting the hidden time structure. *Biophysical Journal*, *88*, L33–L36.

Digman, M. A., Wiseman, P. W., Choi, C., Horwitz, A. R., & Gratton, E. (2009). Stoichiometry of molecular complexes at adhesions in living cells. *Proceedings of the National Academy of Sciences of the United States of America*, *106*, 2170–2175.

Digman, M. A., Wiseman, P. W., Horwitz, A. R., & Gratton, E. (2009). Detecting protein complexes in living cells from laser scanning confocal image sequences by the cross correlation raster image spectroscopy method. *Biophysical Journal*, *96*, 707–716.

Haustein, E., & Schwille, P. (2007). Fluorescence correlation spectroscopy: Novel variations of an established technique. *Annual Review of Biophysics and Biomolecular Structure*, *36*, 151–169.

Kim, S. A., Heinze, K. G., & Schwille, P. (2007). Fluorescence correlation spectroscopy in living cells. *Nature Methods*, *4*, 963–973.

Magde, D., Elson, E., & Webb, W. W. (1972). Thermodynamic fluctuations in a reacting system—Measurement by fluorescence correlation spectroscopy. *Physical Review Letters*, *29*, 705–708.

Magde, D., Elson, E. L., & Webb, W. W. (1974). Fluorescence correlation spectroscopy. II. An experimental realization. *Biopolymers*, *13*, 29–61.

Petersen, N. O. (1986). Scanning fluorescence correlation spectroscopy. I. Theory and simulation of aggregation measurements. *Biophysical Journal*, *49*(4), 809–815.

Petersen, N. O., Brown, C., Kaminski, A., Rocheleau, J., Srivastave, M., & Wiseman, P. W. (1998). Analysis of membrane protein cluster densities and sizes in situ by image correlation spectroscopy. *Faraday Discussions*, *111*, 289–305.

Petersen, N. O., Höddelius, P., Wiseman, P. W., Seger, O., & Magnusson, K. E. (1993). Quantitation of membrane receptor distributions by image correlation spectroscopy: Concept and application. *Biophysical Journal*, *165*(3), 1135–1146.

Ries, J., Chiantia, S., & Schwille, P. (2009). Accurate determination of membrane dynamics with line-scan FCS. *Biophysical Journal*, *96*, 1999–2008.

Ries, J., Yu, S. R., Burkhardt, M., Brand, M., & Schwille, P. (2009). Modular scanning FCS quantifies receptor-ligand interactions in living multicellular organisms. *Nature Methods*, *6*, 643–645.

Ringstad, N., Nemoto, Y., & De Camilli, P. (2001). Differential expression of endophilin 1 and 2 dimers at central nervous system synapses. *The Journal of Biological Chemistry*, *276*, 40424–40430.

Ross, J. A., Chen, Y., Müller, J., Barylko, B., Wang, L., Banks, H. B., et al. (2011). Dimeric endophilin A2 stimulates assembly and GTPase activity of dynamin 2. *Biophysical Journal*, *100*, 729–737.

Schwille, P., Bieschke, J., & Oehlenschläger, F. (1997a). Kinetic investigations by fluorescence correlation spectroscopy: the analytical and diagnostic potential of diffusion studies. *Biophysical Chemistry*, *66*, 211–228.

Schwille, P., Meyer-Almes, F.-J., & Rigler, R. (1997b). Dual-color fluorescence cross-correlation spectroscopy for multicomponent diffusional analysis in solution. *Biophysical Journal*, *72*, 1878–1886.

Schwille, P., Korlach, J., & Webb, W. W. (1999). Fluorescence correlation spectroscopy with single molecule sensitivity on cell and model membranes. *Cytometry*, *36*, 176–182.

Sundborger, A., Soderblom, C., Vorontsova, O., Evergren, E., Hinshaw, J. E., & Shupliakov, O. (2010). An endophilin-dynamin complex promotes budding of clathrin-coated vesicles during synaptic vesicle recycling. *Journal of Cell Science*, *124*, 133–143.